CLM-R228

CLM-R228

UKAEA

Report

THE THERMAL STABILITY AND EQUILIBRIUM OF PERIPHERAL PLASMAS

D. E. T. F. ASHBY
M. H. HUGHES

CULHAM LABORATORY
Abingdon Oxfordshire

1982

C/18

Available from H. M. Stationery Office

£2.00

CLM-R 228

THE THERMAL STABILITY AND EQUILIBRIUM OF PERIPHERAL PLASMAS

D E T F Ashby and M H Hughes
Culham Laboratory, Abingdon, Oxon, OX14 3DB, UK
(Euratom/UKAEA Fusion Association)

ABSTRACT

This paper deals with the thermal stability and equilibrium of a confined plasma when impurity radiation is the dominant loss mechanism near the edge. The energy transport in this peripheral region can be approximately described by the equation

$$3\frac{\partial n_e T}{\partial t} = \frac{\partial}{\partial x}\kappa\frac{\partial T}{\partial x} - n_e n_z L(T)$$

which is shown to be stable as long as the electron density n_e, the impurity density n_z, the thermal conductivity κ and the radiation function L are all functions of T alone and thus do not depend explicitly on x. By contrast, instability is possible if n_e increases linearly with distance and occurs if more than about half the power conducted into the edge region is radiated. These simple results are demonstrated and extended by 1-D computer modelling of INTOR with iron in coronal equilibrium as the impurity. In addition non-coronal effects are examined by modelling the individual charge states of oxygen and allowing them to diffuse; charge-exchange recombination is also included. These additional effects are found to be stabilising.

September 1982

ISBN 0 85311 112 X

CONTENTS

1. INTRODUCTION

The general problem of thermal equilibrium and stability of tokamaks was first considered by Furth et al[1]. More recently, Ohyabu[2,3] and Neuhauser[4] have considered specific equilibrium and stability problems posed by a tokamak with a strongly radiating peripheral region. This note also deals with the peripheral plasma. It considers the thermal stability and equilibrium of this region when impurity radiation is the major loss mechanism and hence complements the work described in ref [5] which dealt with loss of equilibrium alone and did not consider stability.

2. THEORY

If energy is conducted into the peripheral region of a confined plasma where it can be lost by impurity radiation then the energy equation for the peripheral plasma becomes

$$3 \frac{\partial n_e T}{\partial t} = \frac{\partial}{\partial x} \kappa \frac{\partial T}{\partial x} - n_e n_z L(T) \qquad (1)$$

where n_e = electron density,
n_z = impurity density,
κ = thermal conductivity,
$L(T)$ = radiation function,

and for simplicity it has been assumed that $T_i = T_e$ and $n_e = n_i >> n_z$.

2.1 Linear Perturbation Analysis

Consider the stability of eq(1). To generalize let n_e, n_z and κ all be explicit functions of T but <u>not</u> of x; under this assumption a simple condition for thermal stability can be derived as follows by perturbation analysis.

If an equilibrium temperature profile is slightly perturbed then to first order eq(1) gives

$$3\left(n_e + T\frac{dn_e}{dT}\right)\gamma\tilde{T} = \frac{\partial^2}{\partial x^2}(\kappa\tilde{T}) + \left[\frac{d}{dT}(n_e n_z L)\right]\tilde{T} \qquad (2)$$

for a perturbation of the form $\tilde{T} = \tilde{T}(x)\exp\gamma t$. Multiply eq(2) by $\kappa(T)\tilde{T}dx$ and integrate from the plasma boundary (point 'o') to some point within the plasma (point '1'); hence

$$3\gamma\int_0^1 \kappa\left[n_e + T\frac{dn_e}{dT}\right]\tilde{T}^2\,dx = \int_0^1 \kappa\tilde{T}d\left(\frac{\partial\kappa\tilde{T}}{\partial x}\right) - \int_0^1 \frac{(\kappa\tilde{T})^2}{\kappa dT/dx}\,d(n_e n_z L) \qquad (3)$$

and the system is thermally stable if $\gamma < 0$, namely when the righthand side of eq(3) is negative. The two terms on the right can be put into a more suitable form by integrating both by parts and then substituting the equilibrium solution into the second term, thus giving the following condition for stability

$$\left[\kappa\tilde{T}\frac{d(\kappa\tilde{T})}{dx}\right]_0^1 - \left[\frac{\kappa n_e n_z L\tilde{T}^2}{dT/dx}\right]_0^1 - \int_0^1 \left\{\frac{\partial(\kappa\tilde{T})}{\partial x} - \frac{(n_e n_z L)(\kappa\tilde{T})}{\kappa dT/dx}\right\}^2 dx < 0 \qquad (4)$$

Consider the significance of eq(4). The integral term is always stabilizing; even if there was a temperature dependent source, such as ohmic heating, it would still be stabilizing. The only scope for instability lies with the first two terms which are determined by the boundary conditions on the temperature perturbation $\tilde{T}$. The normal boundary constraints keep the heat flux at point 1 constant and make $\tilde{T}_o$ zero; thus the system is stable.

The above analysis has assumed that the parameters are all functions of T and not x. If the analysis is repeated with x-dependence then extra terms appear and no simple conclusions can be drawn; however in the next section we show how some effects of an x-dependence can be deduced by inspection of the equilibrium profiles.

2.2 Equilibrium Profiles and Stability

Consider two simple cases, firstly the case where κ, n_e and n_z are all constant so that the equilibrium profile is given by

$$d^2T/dx^2 = (n_e n_z/\kappa)L(T) \qquad (5)$$

and secondly the case where n_z and κ are still constant but n_e increases linearly with distance with $n_e(0) = 0$ so that

$$d^2T/dx^2 = x(n_e' n_z/\kappa)L(T) \qquad (6)$$

where $n_e' = dn_e/dx$ = constant.

Figure 1 shows numerical solutions of eqs(5) and (6) for the case of iron impurity in coronal equilibrium; values for the functions L(T) were taken from ref [6]. Both equations could be

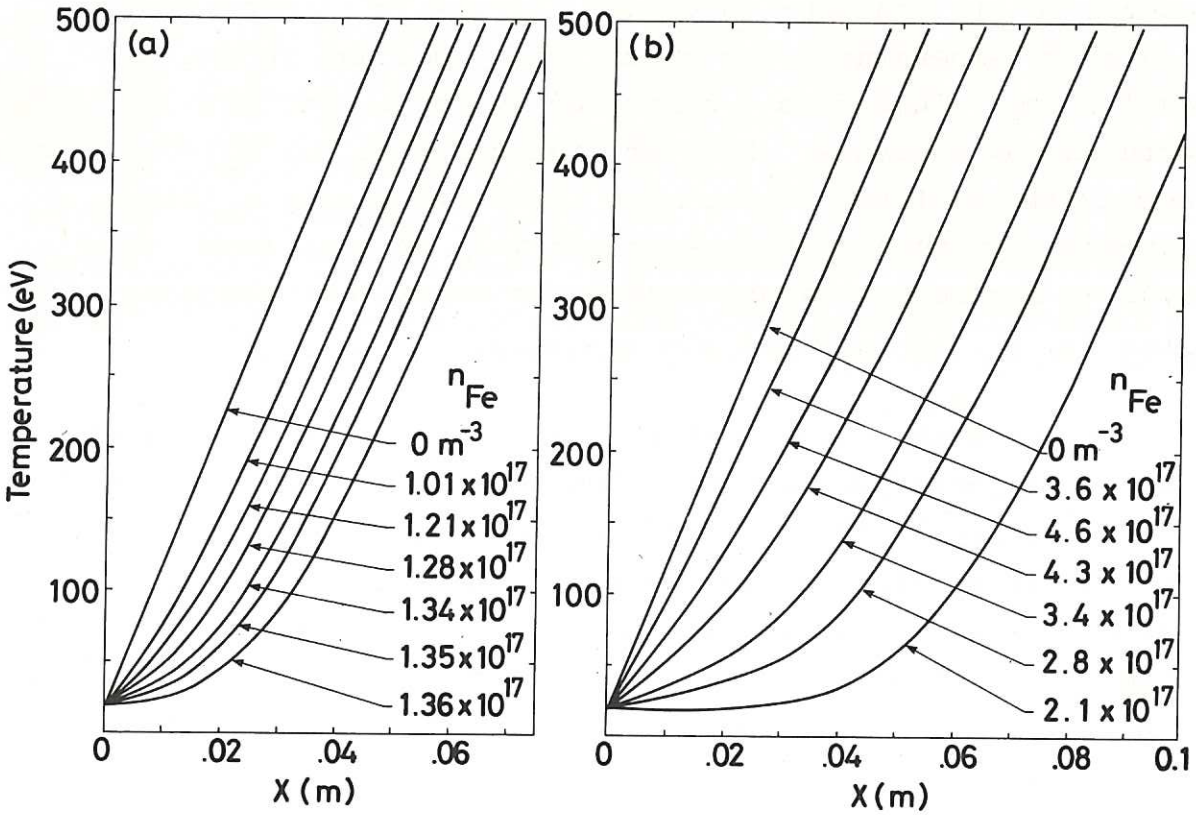

Fig.1 Equilibrium temperature profiles for:–
(a) constant $n_e = 5 \times 10^{19}$ m^{-3}
(b) constant $dn_e/dx = 5 \times 10^{20}$ m^{-4}
The impurity is iron and the plasma parameters are $(dT/dx)_1 = 10^4$ eV/m: $T_o = 20$eV: $\kappa = 5 \times 10^{19}$ m^{-1} s^{-1}.

generalised by incorporating the constant bracketted terms into new distance variables but for convenience the results are plotted for typical values of n_e, n_e', n_z and κ; the curves can easily be scaled to different values of these parameters. The boundary conditions used are

$$(dT/dx)_1 = 10^4 \text{ eV/m}$$

$$T_o = 20 \text{ eV}.$$

Some conclusions on the stability of these profiles can be drawn by inspection alone. Consider the case where n_e is constant; if n_z is increased then the temperatures everywhere are always reduced. Now, suppose that the temperature profile is perturbed to a neighbouring profile at slightly lower temperatures. The value of n_z on the perturbed profile will be too small for equilibrium; consequently the energy input will exceed the radiated power and the plasma will heat up until it returns to its equilibrium value. Similarly if perturbed to higher temperatures the plasma will cool and return to equilibrium. This stable behaviour is consistent with the linear perturbation analysis. However, the profiles for n_e' = constant show a different behaviour; the impurity density n_z first increases and then decreases as $(dT/dx)_0$ is increased. The physical argument used previously now shows that for some values of n_z the profiles are unstable.

Figure 2 shows the curves in Fig. 1 plotted in a general and more informative fashion. The temperature gradient at the inner boundary is plotted against the fraction of power radiated, with the temperature at the inner boundary as a parameter. Simple physical reasoning shows that the profiles are unstable whenever the slope of these curves is positive. Hence the case with constant density is always stable but the case with constant density gradient becomes unstable whenever the radiated power exceeds roughly half the input power irrespective of the values of the plasma parameters. This result highlights a possible difficulty in establishing the 'cold plasma mantle' proposed for JET[7].

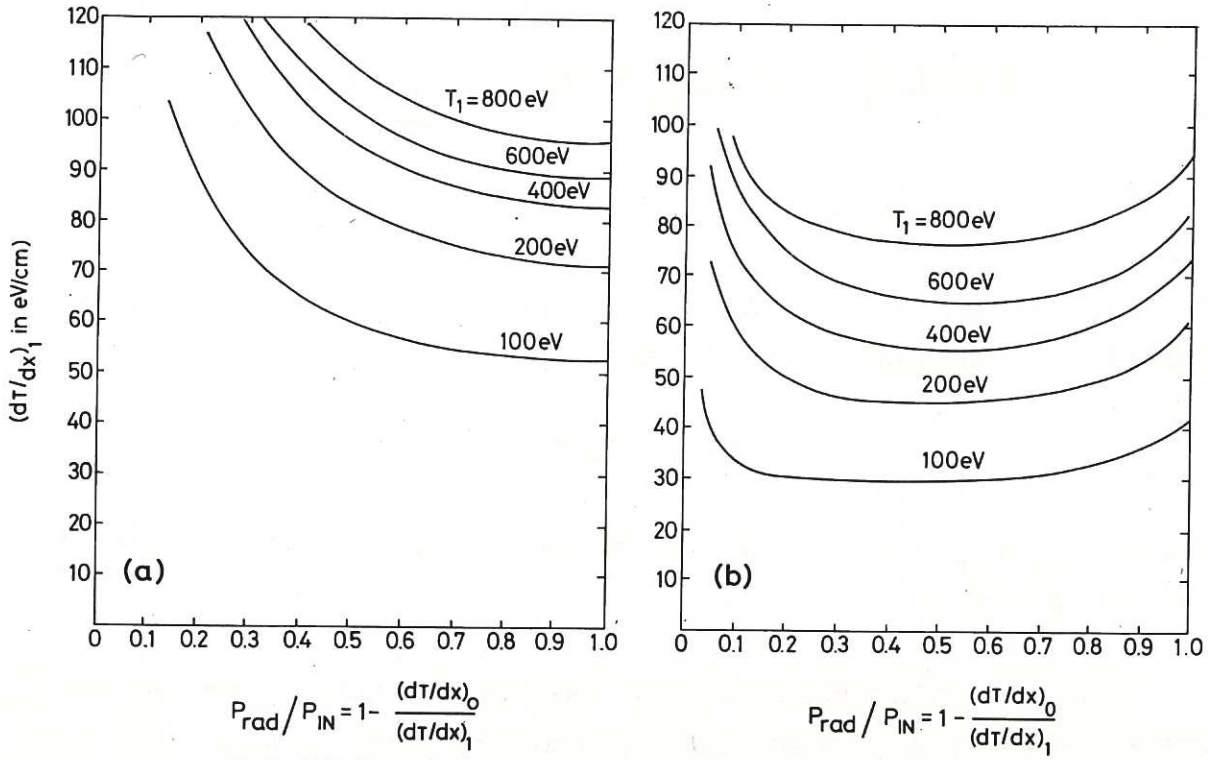

Fig.2 Solutions of
(a) $\kappa d^2T/dx^2 = n_e n_z L(T)$ with $n_e = 5 \times 10^{19}\ m^{-3}$
(b) $\kappa d^2T/dx^2 = x(dn_e/dx) n_z L(T)$ with $dn_e/dx = 5 \times 10^{20}\ m^{-4}$
The impurity is iron and the plasma parameters are
$n_z = 10^{17}\ m^{-3}$: $\kappa = 5 \times 10^{19}\ m^{-1}\ s^{-1}$.

The curves in Fig. 2 depend on the choice of L(T). Insight into the generality of the results is helped by choosing a simple analytic form for the radiation function L(T). A convenient choice is a delta function such that

$$L(T) = 0 \text{ if } T \neq T_{rad}$$

and

$$\int_0^\infty L(T) = I$$

The resulting temperature profile has a constant gradient which changes discontinuously at $T = T_{rad}$. The energy equation for the constant density gradient case (eq(6)) can be integrated to give

$$(dT/dx)_1^2 - (dT/dx)_0^2 = (2n_e'n_z/\kappa)\int_0^1 xLdT$$

$$= (2n_e'n_z/\kappa)(I\ T_{rad}/(dT/dx)_0) \qquad (7)$$

Differentiating with respect to n_z shows that the temperature profile is marginally stable when

$$(dT/dx)_1/(dT/dx)_0 = \sqrt{3}$$

Hence $P_{rad}/P_{in} = 1 - 1/\sqrt{3} = 0.423$ which is consistent with the curves in Fig. 2.

The preceding results have assumed that n_z, κ and n_e or n_e' are constants; the results are, however, more general and this assumption can be relaxed. Suppose that the plasma parameters are not constants but are functions of T. Then for the case of constant density the energy equation is

$$\frac{\partial}{\partial x}\left(\kappa(T)\frac{\partial T}{\partial x}\right) = n_e(T)n_z(T)L(T) \qquad (8)$$

which can be integrated to give

$$Q_1^2 - Q_0^2 = 2\int_0^1 \kappa(T)n_e(T)n_z(T)L(T)\ dT \qquad (9)$$

$$= 2\kappa_o\ n_{e_o}\ n_{z_o} \int_0^1 F(T)\ dT$$

κ_o, n_{e_o} and n_{z_o} are constants and $Q = \kappa\partial T/\partial x$ is the thermal flux.

From eq(9) it follows that $dQ_1/d(P_{rad}/P_{in})$ is always negative, as in Fig.2, and as before the plasma is stable. This result is consistent with the result of the perturbation analysis in the previous section.

On the other hand if $n_e = n'_e x$, where n'_e is a function of T alone, then the energy equation integrates to give

$$Q_1^2 - Q_0^2 = 2\int_0^1 x\kappa(T)n'_e(T)n_z(T)L(T)\ dT$$

$$= 2\ {}_o\, n'_{e_o}\ n_{z_o}\int_0^1 x\ G(T)\ dT \qquad (11)$$

and then, as long as G(T) can be approximated to a delta function, the previous argument holds and the plasma still becomes thermally unstable when roughly half the power is radiated.

3. RESULTS FROM COMPUTATIONAL MODELLING

The previous section derived a condition for the thermal stability of the peripheral region of a confined plasma, namely, that instability ensues when roughly half the power conducted into the peripheral region is radiated. In deriving this result κ, n_z and dn_e/dr were taken as constant. Although this assumption may be questioned it is roughly in line with the assumptions made in the computational models used to predict tokamak behaviour; with this point in mind the 1-D Code HERMES[8] has been used to check and extend the predictions of the previous section by modelling a large tokamak with impurity radiation as a major loss mechanism.

3.1 The Computer Model

Basically the machine parameters and the transport used are the original INTOR reference values as listed in ref [5]; they are summarized below.

The Machine

Major radius	$R = 4.5$ m
Equivalent minor radius	$a = 1.5$ m
Toroidal current	$I = 4$ MA
Toroidal magnetic field	$B_\phi = 5$ tesla

An atomic mass of 2.5 is normally used to simulate a DT-mixture.

Plasma Transport

Electron thermal diffusivity	$\chi_e = \kappa_e/n_e = 5 \times 10^{19}/n_e m^2 sec^{-1}$
Ion thermal diffusivity	$\chi_i = 3 \times$ (the neoclassical value)
Plasma diffusivity	$D = \chi_e/4$ + neoclassical transport including the Ware effect.

Neutral Hydrogen

Unless otherwise stated an influx of neutral DT-mixture into the plasma is modelled. The atoms are arbitrarily given an energy of 30 eV and transported and deposited within the plasma using a Monte Carlo method. Normally the flux is continually adjusted so that ionization just balances the loss of hydrogen by diffusion, (ie a recycling co-efficient of unity).

Power Sources

To simulate auxiliary heating a 10 MW source feeds energy to the central plasma and for simplicity the fusion power is omitted although the ohmic power ($\sim$ 1 MW) is included. This power level is less than that representative of INTOR (50 - 100 MW); the reason for choosing a low power is to decrease the temperature gradient and thus increase the number of computational cells describing the peripheral region.

Impurities

The impurity modelled in this work was iron in coronal equilibrium[6]. For ease of comparison with the results obtained in the previous section n_z was normally taken as constant; when the impurities were allowed to diffuse the flux due to anomalous diffusivity was added to the neoclassical flux.

3.2 Results with dn_H/dr Constant

To check the predictions of section 2 the hydrogen ion density gradient was held constant at $10^{20} m^{-4}$ while the code was run to steady-state conditions for different densities of iron impurity. Note that the physics in this computational model includes several features not present in the analysis of the previous section namely:

(a) cylindrical geometry:
(b) separate electron and ion temperatures:
(c) ohmic heating:
(d) neoclassical thermal conductivity in addition to anomalous transport.

Figure 3 clearly demonstrates the predicted loss of equilibrium when roughly half the power conducted into the

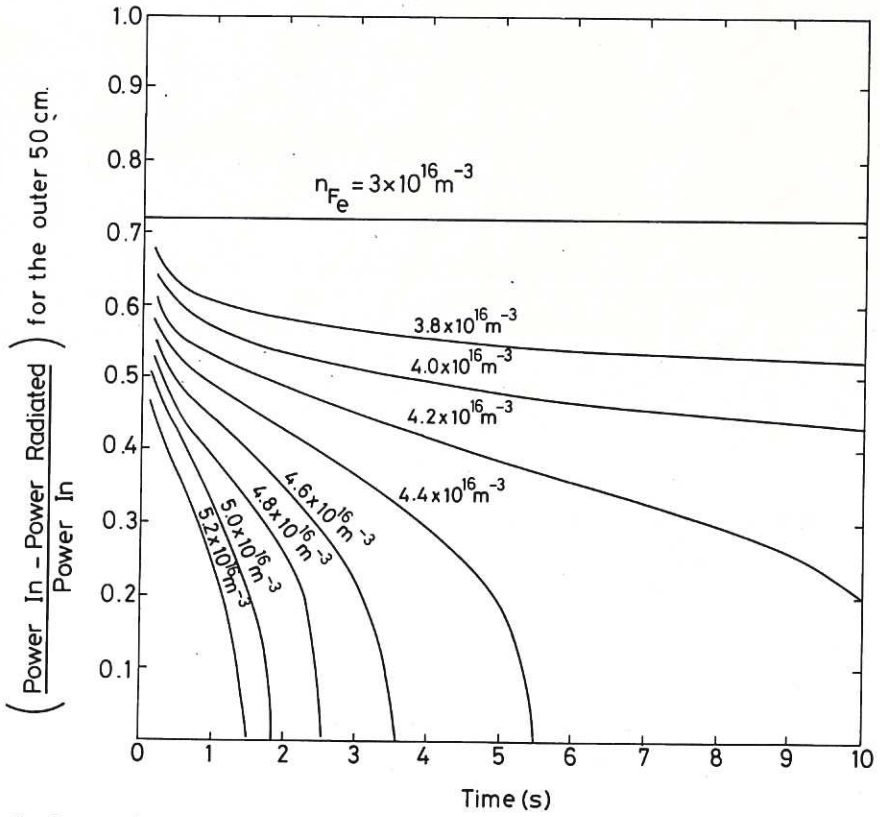

Fig.3 Curves showing the peripheral radiation varies with time when n_z is increased and the density gradient is held constant.
Parameters: Iron impurity: $dn_H/dr = 10^{20} m^{-4}$: INTOR dimensions and reference parameters: 10MW of input power on axis.

peripheral plasma is radiated. To obtain this figure the case with $n_z = 3 \times 10^{16} m^{-3}$ was taken to a steady-state and then used as the initial condition for a series of computations with larger impurity densities; these computations show how the power radiated from the peripheral region (the outer 60 cm) varies with time. With $n_z \leq 4 \times 10^{16} m^{-3}$ a steady-state is always reached in which less than 60% of the input power is radiated; however, at higher impurity densities equilibrium is no longer possible and the radiated power increases until it exceeds the input power when the temperature profile starts to collapse. This result is in complete agreement with the prediction in section 2.

Details of the temperature profile collapse are shown in Figs. 4 and 5 for the case when n_z is increased from $3 \times 10^{16} m^{-3}$

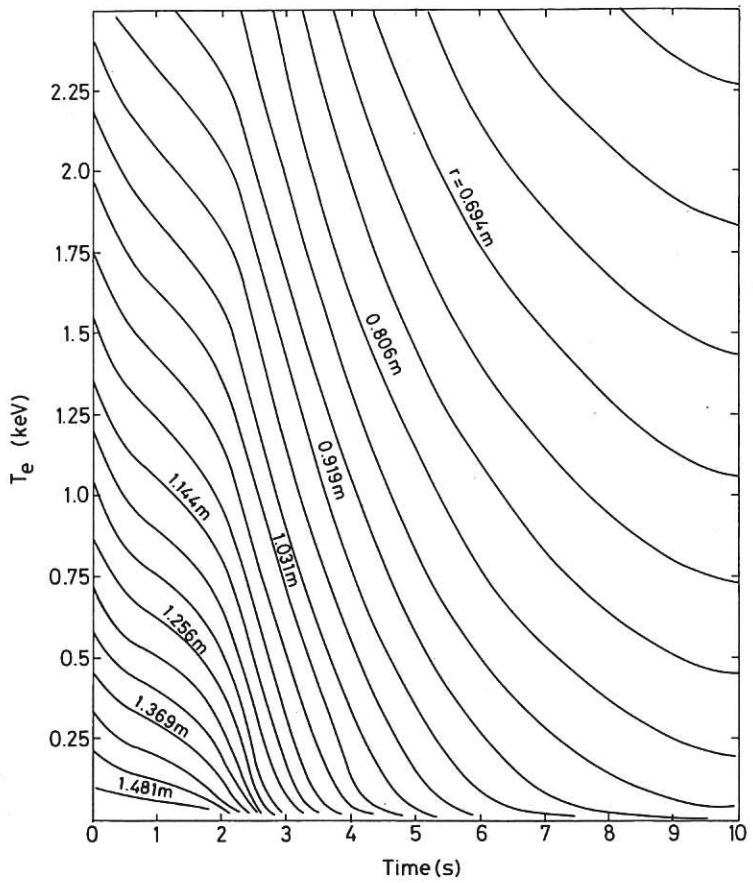

Fig.4 Variation of the peripheral temperatures when the density gradient is held constant. The example shown is where n_z is increased from 3×10^{16} m^{-3} to 5×10^{16} m^{-3} in Fig.3.

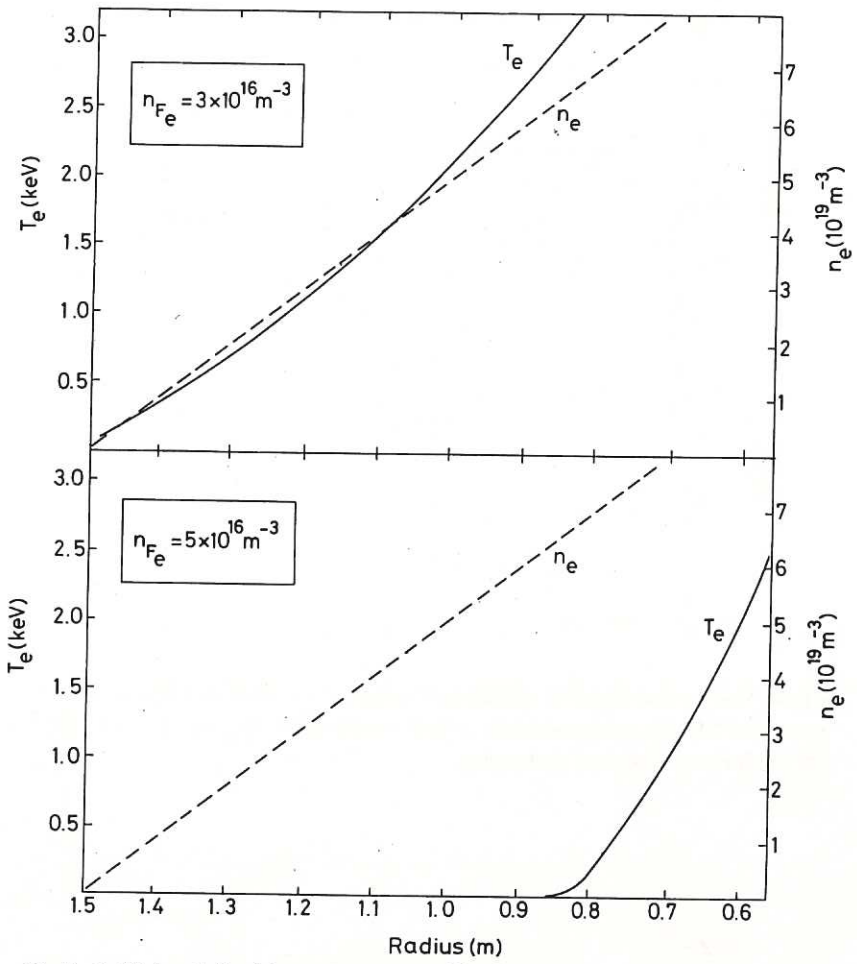

Fig.5 Initial and final temperature profiles for the case illustrated in Fig.4.

to 5 x $10^{16}m^{-3}$. The first of these two figures shows the temporal variation of T_e at points in the peripheral plasma (actually the individual computational cells); the second figure compares the initial and final temperature profiles. The final steady-state is determined mainly by the effect of cylindrical geometry.

3.3 Results with a Self-consistent Density Profile

Having seen that loss of equilibrium occurs as predicted if the density gradient is held constant the computer simulation was repeated with the density determined self-consistently by an influx of neutral hydrogen. Figures 6, 7 and 8 illustrate what happens when $\langle n_H \rangle$ is kept constant in this way at 2 x $10^{19}m^{-3}$ and the impurity density is changed.

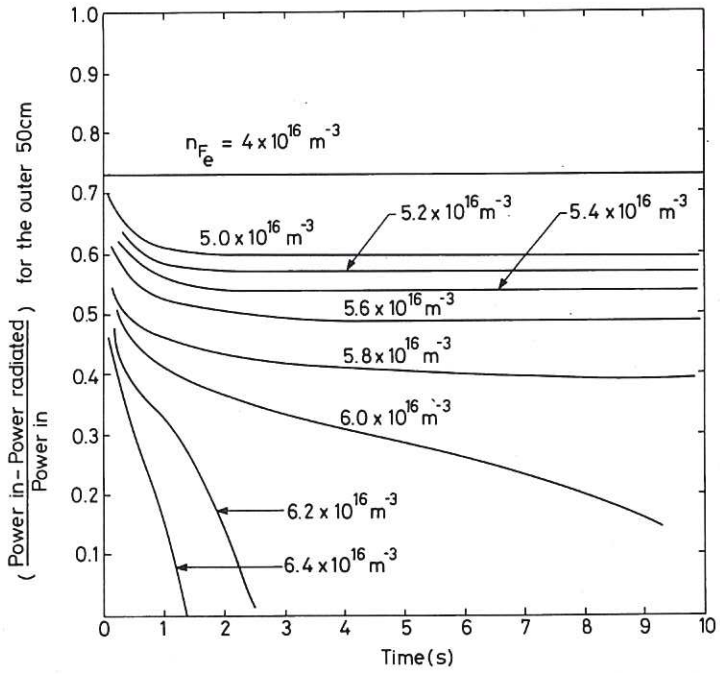

Fig.6 Curves showing the variation of peripheral radiation when n_z is increased and the plasma density is held constant at $<n_H> = 2 \times 10^{19}\ m^{-3}$ by the influx of neutral hydrogen.

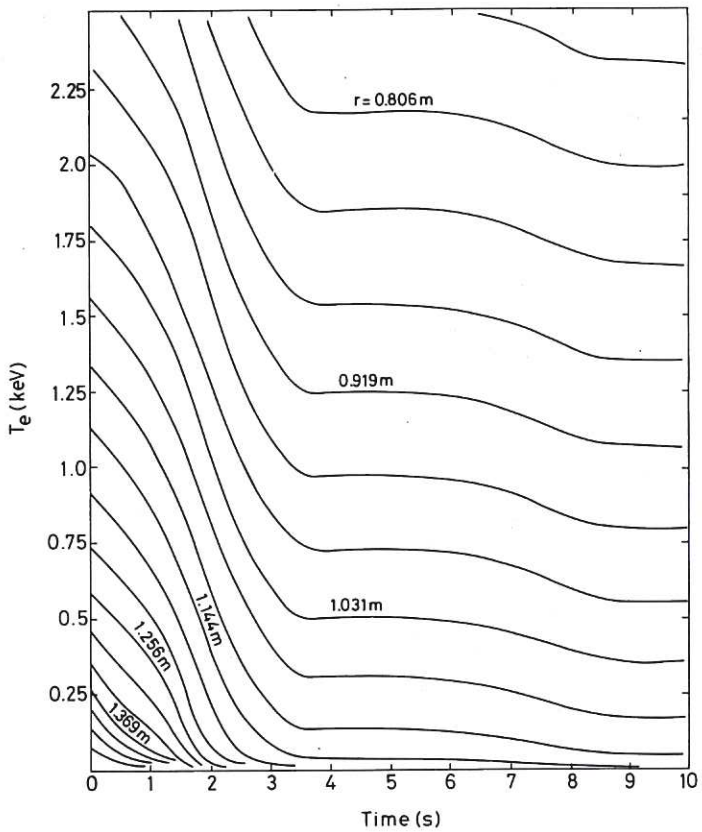

Fig.7 Variation of the peripheral temperatures when $<n_H>$ is kept constant at $2 \times 10^{19}\ m^{-3}$ by the influx of neutral hydrogen and n_z is increased from $4 \times 10^{16}\ m^{-3}$ to $6.4 \times 10^{16}\ m^{-3}$.

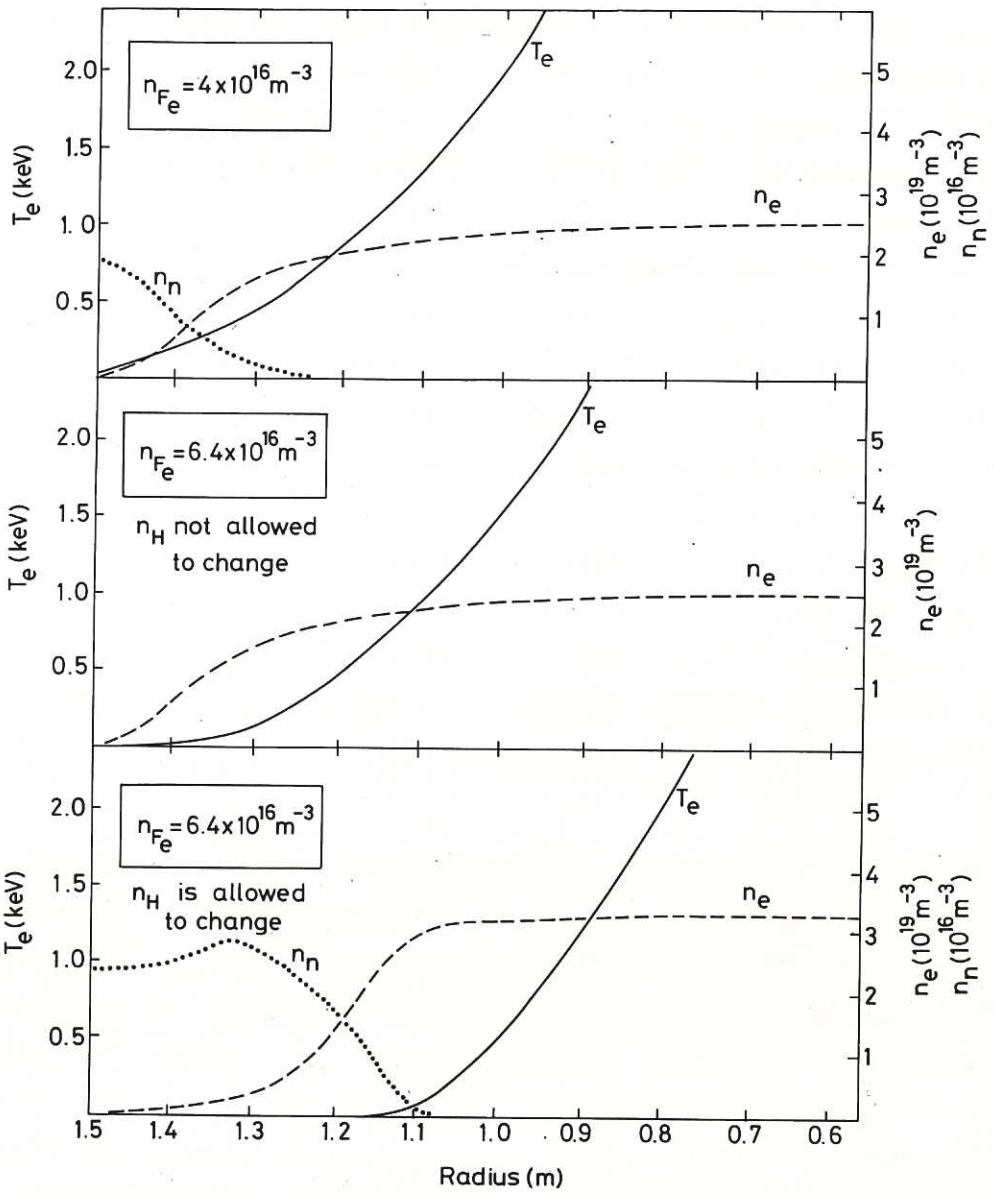

Fig.8 Initial and final profiles of temperature, electron density and neutral density for the case illustrated in Fig.7. Two sets of final profiles are shown; in the first the electron density profile was not allowed to change.

CLM-R 228

Figure 6 shows that as before equilibrium is lost when about 60% of the power transported into the peripheral region is radiated. (In this case convective transport is included.) Figure 7 shows how the peripheral temperatures change with time and Fig. 8 shows the initial and final profiles of density and temperature both when n_e is allowed to change and when it is held constant.

The general behaviour is much the same as before but there is one important difference - the extent of the temperature collapse and the final steady-state are now determined by the way the density profile changes with time. Figure 8 makes this point. When the density profile is not allowed to change the temperature collapse ceases once the low temperature region ($T_e \lesssim 50$ eV) reaches a point on the density profile where the gradient is rapidly decreasing (the minimum of d^2n_e/dr^2). If, however, the density profile is allowed to change self-consistently then the minimum of d^2n_e/dr^2 moves inwards and the temperature collapse continues until a steady-state is reached which is determined by the complex interplay between ionization, neutral transport, plasma transport and thermal transport; unlike the case with a constant density gradient the final steady-state is no longer determined mainly by the effects of cylindrical geometry.

The width of the region in which dn_e/dr is approximately constant depends upon $\langle n_e \rangle$. As the plasma density is increased this width is reduced and eventually it becomes so narrow that the destabilising effect of the density gradient is suppressed; this point is illustrated by Figs. 9 and 10. These two figures, like the previous three figures, refer to the case of a self-consistent density profile but $\langle n_e \rangle$ has been increased from $2 \times 10^{19} m^{-3}$ to $5 \times 10^{19} m^{-3}$ and, as a result, the peripheral region only loses equilibrium when all the power transported from the central region is radiated. This fact is apparent from Fig. 9 which shows how the radiated power varies with time when n_z is changed; stable equilibria result until $n_z \gtrsim 2.1 \times 10^{16} m^{-3}$ when equilibrium becomes impossible since the radiated power exceeds the available power. Figure 10 shows profiles of n_e, n_n and T_e for three of these equilibria. Note how the point where d^2n_e/dr^2 is a minimum occurs at $T_e \lesssim 50$ eV once $n_z > 1.7 \times 10^{16} m^{-3}$ and instability might be expected.

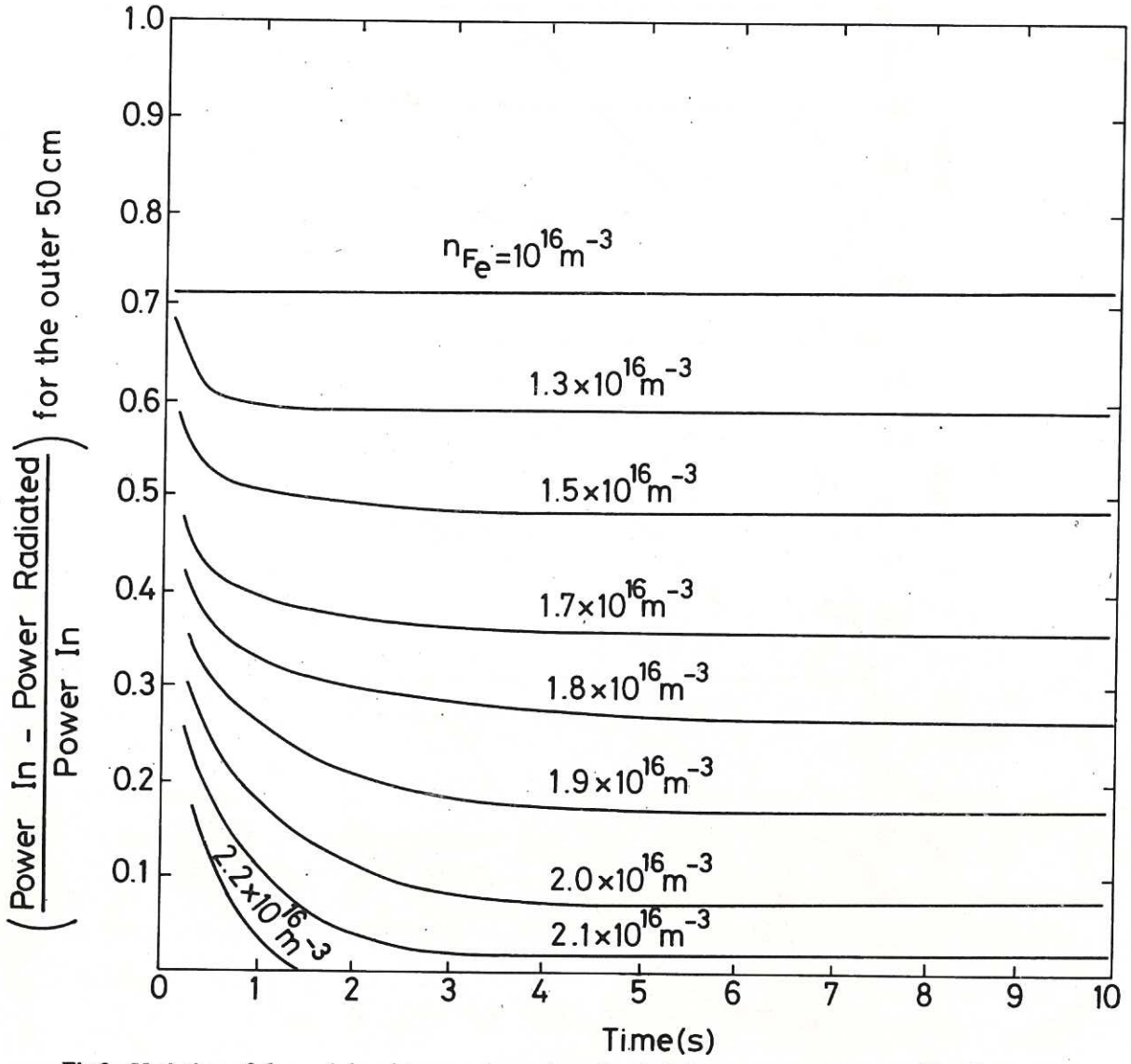

Fig.9 Variation of the peripheral temperature when $\langle n_H \rangle$ is kept constant at 5×10^{19} m^{-3}. At this density no instability occurs unlike the case illustrated in Fig.7 where the density is lower.

The effect of a narrow edge region can be neatly demonstrated analytically with the delta function model used in section 2.2. Again assume that $L(T) = 0$ if $T \neq T_{rad}$ but in addition take a density profile that has dn_e/dx constant until $n_e = n_{max}$ when it becomes zero. It follows that the initial temperature collapse, which occurs when roughly half the power is radiated, ceases when

$$(dn_e/dx)_o/n_{max} < (2/3\sqrt{3})(dT/dx)_1/T_{rad} \qquad (12)$$

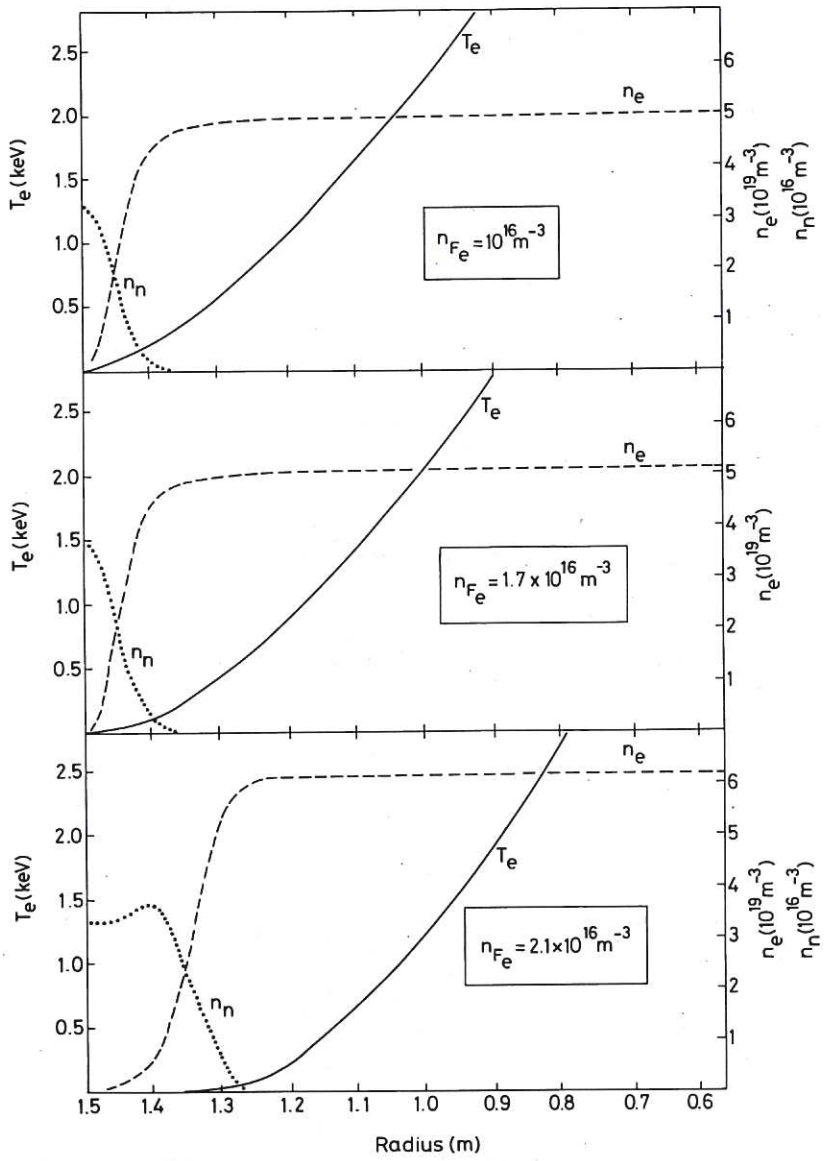

Fig 10 Equilibrium profiles of temperature, electron density and neutral density for three of the cases shown in Fig.9.

The stabilizing influence of a narrow edge region explains why instability was not observed in the situations modelled in ref. 5 where the density of iron impurity was adjusted so that all the input power was radiated. (See Fig. 9(a) ref. 5).

3.4 The Effect of 'Non-coronal' Radiation Models

The results described so far have all assumed that the impurity causing the radiation is iron in 'coronal' or 'ionization' equilibrium so that the charge-state distribution of the impurity is given by

$$\alpha_j n_j = \beta_{j+1} n_{j+1} \qquad (13)$$

where n_j is the density of the j^{th} charge state
α_j is the ionization coefficient of the j^{th} state
β_j is the recombination coefficient of the j^{th} state

In practice the peripheral radiation from tokamaks is often dominated by radiation from the light elements oxygen and carbon which are not normally in 'coronal' equilibrium; the charge-state distribution is affected both by transport and by charge-exchange recombination with neutral hydrogen. In this situation the charge-state distribution is determined from the following rate equation

$$\frac{\partial n_j}{\partial t} + \frac{\partial \Gamma_j}{\partial x} = n_e\left\{n_{j-1}\alpha_{j-1} - (\alpha_j + \beta_j)n_j + n_{j+1}\beta_{j+1}\right\} + n_n\left\{\gamma_{j+1}n_{j+1} - \gamma_j n_j\right\} \qquad (14)$$

where Γ_j is the flux of the j^{th} state
γ_j is the charge-exchange recombination coefficient
n_n is the density of neutral hydrogen.

The effect of taking into account diffusion of the individual charge states and charge-exchange recombination has been investigated using HELIOS[8]. This 1-D code follows the transport of individual charge states and was used to model a slab plasma representing the edge region. The temperature and electron density were calculated self-consistently with the density profile determined by the influx of neutral hydrogen. The conclusions are illustrated by Fig. 11 which shows results for a peripheral plasma with the following parameters.

Thermal conductivity $\kappa = 5 \times 10^{19} m^{-1} s^{-1}$.
Particle diffusivity $D = 0.25\ m^2 s^{-1}$.
Mean plasma density $\langle n_e \rangle = 2.2 \times 10^{19} m^{-3}$.
Power input $= 3.2 \times 10^4\ W/m^2$ $\quad dT/dx = 4\ keV\ m^{-1}$.

The impurity is oxygen and its density is held constant by an influx of O^{+1} at the T=0 boundary.

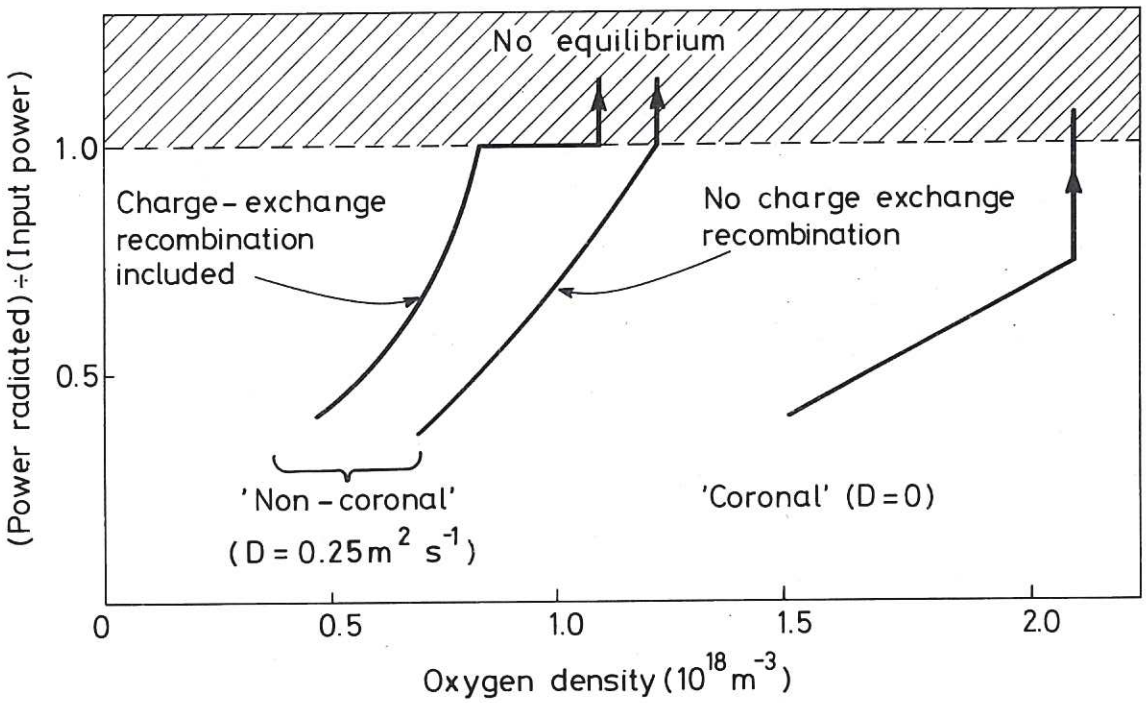

Fig.11 Radiated power as a function of oxygen density for three radiation models. Plasma parameters $\langle n_e \rangle = 2.2 \times 10^{19}\,m^{-3}$, $\kappa = 5 \times 10^{19}\,m^{-1}\,s^{-1}$, $D = 0.25 m^2\,s^{-1}$, $(dT/dx)_l = 4 keV\,m^{-1}$.

CLM-R 228

Figure 11 shows the fraction of power radiated as a function of impurity density for three radiation models. In the first model the charge states of oxygen are not allowed to diffuse hence 'coronal equilibrium' ensues and, as in Fig. 6, the plasma loses equilibrium before the radiated power exceeds the input power. In the second case the charge states can diffuse and the thermal instability is suppressed by the continual change of L(T); however equilibrium is rapidly lost once all the power is radiated. (Note that the difference in critical impurity density between the 'coronal' and 'non-coronal' models is only a factor of two or so; this is in accord with the arguments in ref. [9].) Finally in the third radiation model charge-exchange recombination between the oxygen ions and neutral hydrogen is included with diffusion. Now the plasma exhibits a reluctance to lose equilibrium when radiating all the input power; this phenomenon is related to the finite penetration distance of the hydrogen atoms. Again note that the critical impurity density is not greatly different from the previous two cases.

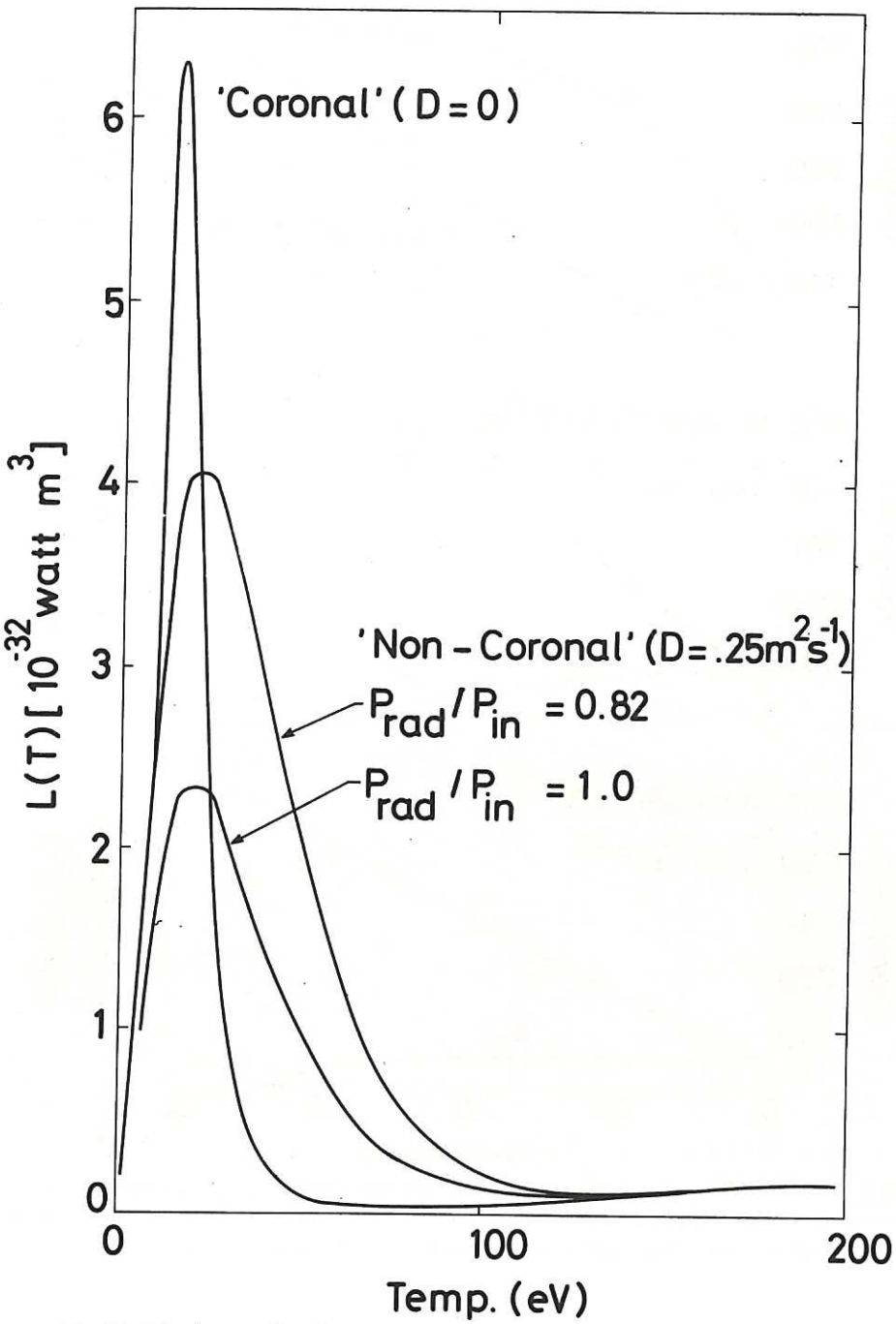

Fig.12 The 'coronal' radiation function compared with radiation function at two power levels when D = 0.25 $m^2 s^{-1}$ (see Fig.11) charge-exchange recombination is not included.

Figures 12 and 13 illustrate why the two 'non-coronal' models exert a stabilising influence. Figure 12 shows how L(T) is reduced as the power radiated is increased by adding more oxygen. This progressive reduction is brought about by charge-state diffusion which becomes less important as dT/dx is decreased by radiation so that L(T) tends to move towards the coronal value (see ref. 9).

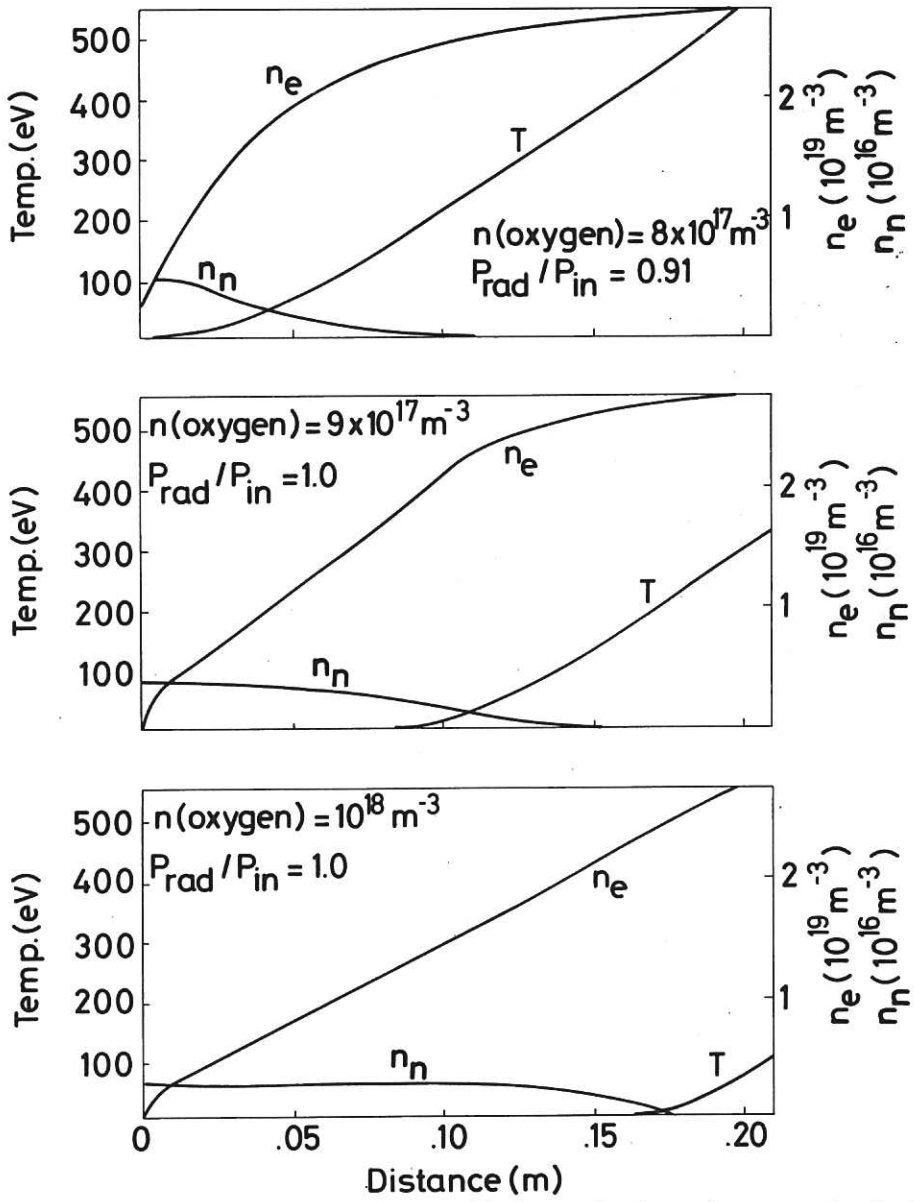

Fig.13 Profiles of n_e, T_e and n_n, the neutral hydrogen density as the oxygen density is increased and the temperature profile attempts to collapse (see Fig.11). Charge-exchange recombination is included together with charge-state diffusion ($D = 0.25\,m^2\,s^{-1}$).

Figure 13 explains why charge-exchange recombination between oxygen ions and neutral hydrogen has the effect shown in Fig. 11. Although the neutral hydrogen penetrates further into the plasma as the temperature collapses the neutral density at any specific temperature decreases; hence the enhancement of L(T) caused by charge-exchange recombination steadily decreases. Finally as the enhancement approaches zero thermal equilibrium is lost and the temperature profile collapses.

Note that according to Fig. 11 the increase in radiation as a result of charge exchange recombination is quite small (less than a factor of two). This result is at variance with the results of Hulse et al [10] who predict orders of magnitude changes in L(T) for oxygen once $n_n/n_e \gtrsim 10^{-4}$. The difference results from charge-state diffusion, which is not included in ref. 10; the difference is easily understood from the following argument. If the charge states cannot diffuse then charge-exchange recombination has a marked effect once it becomes comparable with ordinary recombination since, in this case, relative abundances are determined by

$$\alpha_j n_j = (\beta_{j+1} + \gamma_{j+1}\, n_n/n_e)\, n_{j+1} \qquad (15)$$

instead of eq.13. However, once diffusion is large enough, equilibrium is no longer determined by a balance between ionization and recombination but by a balance between ionization and transport instead (see eq.14). In this situation normal recombination is unimportant and charge-exchange recombination must compete with the potentially larger ionization terms if it is to affect the distribution of charge states and hence the radiation function L(T).

3.5 Feedback Between n_z and the Peripheral Plasma

The results described so far have assumed that the impurity density n_z is constant throughout the plasma and does not vary with time. In practice the main source of impurity will be the wall and the plasma limiter and therefore the impurity concentration can be expected to depend upon the properties of the peripheral plasma which are in turn dependent upon the impurity concentration.

The effect of coupling the impurity concentration and the parameters of the edge plasma was investigated by extending the work described in section 3.3, namely by using HERMES to model a tokamak with iron in coronal equilibrium as the impurity. The production of impurities was assumed to depend upon the 'non-radiative' losses from the plasma. Three methods of feed-back were tried.

(1) The impurity level was changed instantaneously in proportion to the non-radiative losses.

(2) The density of iron at the plasma boundary was made proportional to the non-radiative losses; within the plasma the iron ions were allowed to diffuse (see section 3.1).

(3) The flux of neutral iron into the plasma was made proportional to the non-radiative losses. The neutral iron was then ionised and allowed to diffuse as before.

Irrespective of the method of feed-back and the magnitude of the constant of proportionality used the edge region settled into a stable equilibrium with most of the power radiated; this result is in direct contrast to the other results described and suggests that temperature collapse will not occur.

4. DISCUSSIONS AND CONCLUSIONS

We have considered theoretically the effect of impurity radiation on the thermal equilibrium and stability of the peripheral plasma of a tokamak and seen that instability and loss of equilibrium can occur; we have also seen that diffusion of the different impurity charge states, charge-exchange recombination and feedback between the impurity level and 'wall loading' are all stabilizing influences - particularly the last. On the basis of this evidence it is tempting to conclude that temperature profile collapse will not occur; this conclusion however, can be challenged on the basis of experimental observation. In some circumstances at least temperature profile collapse does occur.

It is important to appreciate that some potentially relevant aspects of the overall problem have been omitted in the present study; for example the 'scrape-off layer', which in a tokamak exists between the edge of the limiter and the wall, has been ignored. Ohyabu[2] has pointed out that the plasma

temperature of this region plays a major role in determining the energy balance and stability of the peripheral plasma; this point is avoided in the perturbation analysis of section 2.1 by taking the commonly-used boundary condition $\hat{T}_o = 0$. It is easy to see that changing this boundary condition might affect stability since the value of the integral $\int_{T_o}^{T_1} L dT$, which directly affects the power radiated, is very sensitive to T_o in the range 10 - 30 eV when light elements are considered.

Further complications can occur in the scrape-off region which affect the edge temperature and its dynamic behaviour. Proudfoot and Harbour[11] have observed that neutral gas re-cycling and its associated energy loss plays an important role in the behaviour of the 'scrape-off layer' in the DITE tokamak. In addition Howe[12] draws attention to the importance of effects associated with molecular dissociation of the hydrogen gas fed into the 'scrape-off region'.

Finally the transport of the impurity charge states has been over-simplified; the possibility of additional transport terms as predicted by neoclassical theory, has been largely ignored. But then both the thermal transport and the particle transport are liable to be more complicated than has been assumed.

The results presented are incomplete and cannot be taken unreservedly to predict tokamak behaviour; they do, however, bear strongly on the behaviour of the theoretical models currently used to describe tokamaks.

REFERENCES

[1] FURTH, H. P., ROSENBLUTH, M. N., RUTHERFORD, P. H. and STODIEK, W., Phys. Fluids 13 No.12 (1976) 3020.

[2] OHYABU, N., Nuclear Fusion 9 No.11 (1979) 1491.

[3] OHYABU, N., Kakuyogo - Kenkyu, Nuclear Fusion Research 46, No. 1, (1981) 9.

[4] NEUHAUSER, J., 'Characteristics of a Radiating Layer Near the Boundary of a Contaminated Plasma'. Max-Planck Institute for Plasmaphysik IPP1/182 (1980).

[5] ASHBY, D. E. F. T. and HUGHES, M. H., Nuclear Fusion 21 No.8 (1981) 911.

[6] POST, D. E., JENSEN, R. V., TARTER, C. B., GRASBERGER, W. H. and LOKKE, W. A., Atomic Data and Nuclear Data Tables 20 No.5 (1977) 397.

[7] WATKINS, M. L., STRINGER, T. E., GIBSON, A., CORE, W. G. F., ROBERTSON, I. L., CORDEY, J. G. and FIELD, J. J., in Plasma Physics and Controlled Nuclear Fusion Research (Proc. 8th Int. Conf. Brussels, 1980) Vol.1 IAEA Vienna (1981) 639.

[8] Details of HERMES and HELIOS are available on request from M H Hughes.

[9] ASHBY, D.E.T.F. and HUGHES, M.H. in Controlled Fusion and Plasma Physics (Proc 10th Europ. Conf. Moscow 1981) Paper J-10.

[10] HULSE, R.A., POST, D.E. and MIKKELSEN, D.R., J Phys B 13 (1980) 3895.

[11] PROUDFOOT, G and HARBOUR, P.J., 'Observations of Dynamic Changes in Density Gradients and Associated Fluxes in the DITE Boundary Layer' 5th Int. Conf. Plasma Surface Interactions in Controlled Fusion Devices, Gatlinberg (1982) Paper F4

[12] HOWE, H.C. ibid., 'Dependence of Hydrogen Recycling on Molecular Effects in Tokamaks', Paper F33

HER MAJESTY'S STATIONERY OFFICE

Government Bookshops

49 High Holborn, London WC1V 6HB
(London post orders: PO Box 569, London SC1 9NH)
13a Castle Street, Edinburgh EH2 3AR
41 The Hayes, Cardiff CF1 1JW
Brazennose Street, Manchester M60 8AS
Southey House, Wine Street, Bristol BS1 2BQ
258 Broad Street, Birmingham B1 2HE
80 Chichester Street, Belfast BT1 4JY

Publications may also be ordered through any bookseller